Electron-hole binding in a quantum-dot lattice: Excitonic oscillator strength

S. K. Lyo*
Sandia National Laboratories, Albuquerque, New Mexico 87185, USA
and Korea Advanced Institute of Science and Technology (KAIST), Taejeon, South Korea
(Received 18 January 2005; revised manuscript received 16 May 2005; published 13 July 2005)

We study the excitonic oscillator strength and energies arising from the binding of an electron and a hole interacting through an attractive potential in a tunnel-coupled quantum-dot lattice. The effect of interdot tunneling of the electron and the hole and their attraction on the exciton oscillator strength and exciton binding is evaluated in one-dimensional (1D) and two-dimensional (2D) lattices. For short-range interaction, we find that close packing of the quantum dots into a 2D lattice can result in a nearly abrupt loss of electron-hole binding and the oscillator strength in contrast with a 1D lattice, where the effect is gradual. Numerical application includes general electron-hole attraction in 1D lattices and on-site plus nearest-neighbor attraction in 2D lattices. The time-dependent behavior of the oscillator strength is also examined for 1D on-site attraction.

DOI: 10.1103/PhysRevB.72.045322 PACS number(s): 73.20.Mf, 73.21.Cd, 73.21.La, 78.67.−n

I. INTRODUCTION

Excitons are a good storage source of light energy and play an increasingly important role in optoelectronic devices. The physics of excitons in a single confined structure as well as in a regular array of confined structures in semiconductors is of much current interest. In modern devices, dense stacks of quantum dots (QDs), quantum wires, and quantum wells are used to enhance the quantum efficiency. Excitons show interesting properties in quantum wells,[1–7] quantum wires,[8,9] coupled quantum-well and QD structures,[10,11] and QDs.[12–15] With recent advances in the fabrication of a regular array of QDs, it is possible to control the dot size as well as the structure of the QD lattice.[15–18] The excitonic property of a single QD such as the oscillator strength is mainly determined by the confinement effect of the carriers and their Coulomb interaction. In a regular array of QDs, however, interdot tunneling of electrons and holes can significantly affect the energy structure and affect the quantum efficiency such as the oscillator strength.[16,19–22] In this paper, we study how single-dot excitonic properties evolve in a QD lattice due to the competition between the electron-hole attraction which brings the pair closer together and interdot tunneling which moves them away from each other. In particular, we focus on the relative role of the dimensionality and the range of the interaction. The formalism developed here is applied to evaluate these effects in a one-dimensional (1D) QD lattice for general electron-hole interactions, on-site and nearest-neighbor interaction in two-dimensional (2D) lattices, and on-site interaction in three-dimensional (3D) lattices. For short-range interactions, we find that close packing of the QDs into a 2D lattice can result in a nearly abrupt reduction of the binding energy and the oscillator strength in contrast to a 1D lattice, where this effect is more gradual.

II. MODEL HAMILTONIAN AND FORMALISM

The Hamiltonian of an electron and a hole tunneling between the dots in the lattice is given by[22–25]

$$H = H_e^{(0)} + H_h^{(0)} + H', \tag{1}$$

where $H_e^{(0)}$, $H_h^{(0)}$ describe single-particle motion for the electron and hole, respectively, and H' is the electron-hole interaction given in the site representation by

$$H' = \sum_{\mathbf{m},\mathbf{n}_e} V_{\mathbf{m}} a_{\mathbf{n}_e}^{\dagger} a_{\mathbf{n}_e} b_{\mathbf{n}_e+\mathbf{m}}^{\dagger} b_{\mathbf{n}_e+\mathbf{m}}. \tag{2}$$

Here, $a_{\mathbf{n}_e}^{\dagger}$ and $a_{\mathbf{n}_e}$ ($b_{\mathbf{n}_h}^{\dagger}$ and $b_{\mathbf{n}_h}$) are creation and destruction operators for the electron (hole) at a QD at site $\mathbf{n}_e$ ($\mathbf{n}_h=\mathbf{n}_e+\mathbf{m}$) and $V_{\mathbf{m}} \equiv -U_{|\mathbf{m}|}$ (with $U_{|\mathbf{m}|} \geqslant 0$) is the electron-hole interaction. The quantity $|\mathbf{m}|$ is the distance between the electron and the hole. A cubic or a square lattice structure with a unit lattice constant is assumed for simplicity. The present electron-hole problem is reduced to a single-particle problem as will be shown later. The eigenvalues of $H_e^{(0)}+H_h^{(0)}$ are given by

$$(H_e^{(0)} + H_h^{(0)})|\mathbf{k}_e,\mathbf{k}_h\rangle = \varepsilon(\mathbf{k}_e,\mathbf{k}_h)|\mathbf{k}_e,\mathbf{k}_h\rangle, \tag{3}$$

where $\varepsilon(\mathbf{k}_e,\mathbf{k}_h)=\varepsilon_{e,\mathbf{k}_e}+\varepsilon_{h,\mathbf{k}_h}$ and $\mathbf{k}_e,\mathbf{k}_h$ are wave vectors. These energies are given in the tight-binding approximation by

$$\varepsilon_{\alpha,\mathbf{k}_\alpha} = \sum_{\mathbf{m}} 2J_\alpha(\mathbf{m})\cos(\mathbf{k}_\alpha \cdot \mathbf{m}), \tag{4}$$

where $J_\alpha(\mathbf{m})$ is the tunneling integral for an electron ($\alpha=e$) and a hole ($\alpha=h$) between the sites (i.e., QDs) at $\mathbf{n}=\mathbf{0}$ and $\mathbf{n}=\mathbf{m}$. For small QDs, excited levels are far above the ground state. Therefore, only the ground state of the QDs is considered in this paper, although the result can be applied to any QD level.

A numerical study of a similar model based on on-site and nearest-neighbor attraction was given previously[21,22] for several QDs on a 1D chain and a ring. With recent advances in the growth technology, it is possible to stack QDs to make a 1D quantum-dot lattice and stack 1D lattices to make a 2D lattice for device applications. Analytic solutions are possible for such extended systems as will be presented here. It is interesting to see how the electron-hole binding and optical

properties depend on the dimensionality of the array and the range of the interaction. In one dimension, our result is consistent with the earlier numerical result in the long-chain limit.[22] The exciton absorption was also studied numerically for nearest-neighbor tunneling $J_\alpha = J_\alpha(1)$ for a large chain using U_0 for the electron-hole distance $r=0$ and U_1/r for $r \geqslant 1$ and $U_1 = 0.6U_0$.[23] The effect of anisotropic interchain tunneling and attraction in a large 2D square lattice was studied numerically using a similar model for $U_1 = 0.75U_0$ and $U_0 = |J_e(1) + J_h(1)|$.[24]

The intradot Coulomb attraction U_0 is of the order of a few milli-electron-volts for QDs with a diameter of a few tens of nanometers. For an average separation of 20 nm, for example, the intradot electron-hole attraction equals $U_0 = 6$ meV for the bulk dielectric constant $\kappa = 12$. The absolute value of the tunneling integral J_e for the electron is about 1 meV for the $GaAs/Al_{0.3}Ga_{0.7}As$ double well structure with 15 nm widths and a 2.5 nm wide barrier and can be much smaller for wider barriers.[27,28] The absolute value of the tunneling integral J_h for the hole is much smaller due to the heavy mass. The strength of the tunneling integral can vary significantly depending on the material inside the barrier. The electron and hole QD levels under consideration can be any of the QD levels as long as they are separated from other nearest levels by $\gg |J_\alpha|$. This condition is not well satisfied for large QDs, where exciton-exciton many-body problems can become important at a high exciton density. The present study considers only lattices with small dot sizes and is relevant to systems with low exciton densities.

Assume that the electron-hole pair is created at an arbitrary site $\mathbf{n}_e = \mathbf{n}_h = 0$ at time $t=0$. The probability amplitude that the electron and the hole are at sites $\mathbf{n}_e$, $\mathbf{n}_h$ at time $t \geqslant 0$ is then given by[26]

$$G_{\mathbf{n}_e,\mathbf{n}_h}(t) = \langle \mathbf{n}_e, \mathbf{n}_h | \exp(-itH/\hbar) | 0,0 \rangle. \tag{5}$$

Defining

$$G_{\mathbf{n}_e,\mathbf{n}_h}(z) = \frac{1}{i\hbar} \int_0^\infty e^{izt/\hbar} G_{\mathbf{n}_e,\mathbf{n}_h}(t) dt, \tag{6}$$

where z has an infinitesimal positive imaginary part, we find

$$G_{\mathbf{n}_e,\mathbf{n}_h}(z) = \langle \mathbf{n}_e, \mathbf{n}_h | \frac{1}{z-H} | 0,0 \rangle \tag{7}$$

and

$$G_{\mathbf{n}_e,\mathbf{n}_h}(t) = \frac{i}{2\pi} \int_{-\infty}^\infty e^{-izt/\hbar} G_{\mathbf{n}_e,\mathbf{n}_h}(z) dz. \tag{8}$$

Employing a similar definition for the case $H \to H^{(0)} = H_e^{(0)} + H_h^{(0)}$, we find

$$g_{\mathbf{n}_e,\mathbf{n}_h}(z) = \langle \mathbf{n}_e, \mathbf{n}_h | \frac{1}{z-H^{(0)}} | 0,0 \rangle. \tag{9}$$

III. GREEN'S FUNCTIONS

The Green's functions introduced in Eq. (7) in the energy representation can be evaluated using the standard Dyson equation

$$G_{\mathbf{n}_e,\mathbf{n}_h} = g_{\mathbf{n}_e,\mathbf{n}_h} + \sum_{\mathbf{n},\mathbf{n}'} g_{\mathbf{n}_e,\mathbf{n}_h;\mathbf{n},\mathbf{n}'} V_{\mathbf{n}'-\mathbf{n}} G_{\mathbf{n},\mathbf{n}'}. \tag{10}$$

Here, $g_{\mathbf{n}_e,\mathbf{n}_h;\mathbf{n},\mathbf{n}'}$ has a similar definition as in Eq. (9) except that the initial sites of the electron and hole are at $\mathbf{n},\mathbf{n}'$, respectively. In terms of the plane-wave representation

$$|\mathbf{k}_e, \mathbf{k}_h\rangle = \frac{1}{N} \sum_{\mathbf{n}_e,\mathbf{n}_h} \exp(-i\mathbf{k}_e \cdot \mathbf{n}_e) \exp(-i\mathbf{k}_h \cdot \mathbf{n}_h) |\mathbf{n}_e, \mathbf{n}_h\rangle,$$

we find

$$g(\mathbf{k}_e, \mathbf{k}_h) = \frac{1}{N} \sum_{\mathbf{n}_e,\mathbf{n}_h} e^{i\mathbf{k}_e \cdot \mathbf{n}_e} e^{i\mathbf{k}_h \cdot \mathbf{n}_h} g_{\mathbf{n}_e,\mathbf{n}_h} \tag{11}$$

and

$$g(\mathbf{k}_e, \mathbf{k}_h) = \frac{1}{N} \frac{1}{z - \varepsilon(\mathbf{k}_e, \mathbf{k}_h)}, \tag{12}$$

where N is the total number of the lattice sites. The z dependence is suppressed for the simplicity of the notation when there is no confusion. Similarly, we define

$$G(\mathbf{k}_e, \mathbf{k}_h) = \frac{1}{N} \sum_{\mathbf{n}_e,\mathbf{n}_h} e^{i\mathbf{k}_e \cdot \mathbf{n}_e} e^{i\mathbf{k}_h \cdot \mathbf{n}_h} G_{\mathbf{n}_e,\mathbf{n}_h}, \tag{13}$$

$$G_{\mathbf{n}_e,\mathbf{n}_h} = \frac{1}{N} \sum_{\mathbf{k}_e,\mathbf{k}_h} e^{-i\mathbf{k}_e \cdot \mathbf{n}_e} e^{-i\mathbf{k}_h \cdot \mathbf{n}_h} G(\mathbf{k}_e, \mathbf{k}_h).$$

In order to simplify the Dyson equation in Eq. (10), we use the translational-symmetry property $g_{\mathbf{n}_e,\mathbf{n}_h;\mathbf{n},\mathbf{n}'} = g_{\mathbf{n}_e-\mathbf{n},\mathbf{n}_h-\mathbf{n}'}$ and the inversion symmetry, obtaining

$$G(\mathbf{k}_e, \mathbf{k}_h) = g(\mathbf{k}_e, \mathbf{k}_h) \Bigg[1 + \sum_{\mathbf{m}} V_{\mathbf{m}} \sum_{\mathbf{k}'} \cos(\mathbf{k}' \cdot \mathbf{m}) \times G(\mathbf{k}_e + \mathbf{k}', \mathbf{k}_h - \mathbf{k}') \Bigg]. \tag{14}$$

It is convenient to define

$$\Psi_{\mathbf{m}} = \sum_{\mathbf{n}} G_{\mathbf{n}+\mathbf{m},\mathbf{n}} = \sum_{\mathbf{k}} \cos(\mathbf{k} \cdot \mathbf{m}) G(\mathbf{k}, -\mathbf{k}), \tag{15}$$

where the second equality arises from the second equation in Eq. (13). The quantity $\Psi_{\mathbf{m}}$ is related to the probability amplitude where the electron and the hole are separated by $\mathbf{m}$, while the quantity $\Psi_{\mathbf{m}=0}$ yields the oscillator strength as will be shown shortly. Similarly, we define

$$\psi_{\mathbf{m}} = \sum_{\mathbf{n}} g_{\mathbf{n}+\mathbf{m},\mathbf{n}} = \sum_{\mathbf{k}} \cos(\mathbf{k} \cdot \mathbf{m}) g(\mathbf{k}, -\mathbf{k}). \tag{16}$$

The quantity $G(\mathbf{k},-\mathbf{k})$ in Eq. (15) is obtained from Eq. (14) by choosing $\mathbf{k}_e = -\mathbf{k}_h = \mathbf{k}$:

$$G(\mathbf{k}, -\mathbf{k}) = g(\mathbf{k}, -\mathbf{k}) \Bigg[1 + \sum_{\mathbf{m}} V_{\mathbf{m}} \cos(\mathbf{k} \cdot \mathbf{m}) \Psi_{\mathbf{m}} \Bigg], \tag{17}$$

where use is made of the inversion symmetry.

In the self-consistent Eqs. (15) and (17), the entire information from the noninteracting part of the electron and hole Hamiltonian is contained in the quantity $g(\mathbf{k},-\mathbf{k}) = [z$

$-\varepsilon(\mathbf{k})]^{-1}$ in Eq. (17), where $\varepsilon(\mathbf{k}) \equiv \varepsilon(\mathbf{k},-\mathbf{k}) = \varepsilon(\mathbf{k},\mathbf{k}) = \varepsilon_e(\mathbf{k}) + \varepsilon_h(\mathbf{k})$. Thus, the effective motion is given by $J = J_e + J_h$ for a tight-binding model in Eq. (4) with the nearest-neighbor transfer integrals J_e and J_h. This is consistent with an earlier result.[22] In general, we can account for the combined electron and hole motion by replacing the $\mathbf{m}$th nearest electron transfer integral $J_e(\mathbf{m})$ by the effective $J(\mathbf{m}) = J_e(\mathbf{m}) + J_h(\mathbf{m})$ for the effective energy dispersion $\varepsilon(\mathbf{k})$ in view of Eq. (4) and drop the hole motion. For the effective-mass model, this corresponds to introducing the reduced mass: $1/m^* = 1/m_e + 1/m_h$. With this effective $\varepsilon(\mathbf{k})$, we can drop the hole motion, setting $\mathbf{n}_h = 0$ in Eq. (5) and those that follow. The net result is equivalent to replacing the $\mathbf{n}$ summation in Eq. (15) with $\mathbf{n} = 0$.

The quantity $\Psi_{\mathbf{m}}$ in Eq. (15) is then simplified, using Eq. (7), as

$$\Psi_{\mathbf{m}} = G_{\mathbf{m},0} = \sum_{\alpha} \frac{f_\alpha(\mathbf{m})}{z - \varepsilon_\alpha}, \quad f_\alpha(\mathbf{m}) = \langle \mathbf{m},0|\alpha\rangle\langle\alpha|0,0\rangle, \tag{18}$$

where $|\alpha\rangle$ are eigenstates of $H: H|\alpha\rangle = \varepsilon_\alpha|\alpha\rangle$. The poles of $\Psi_{\mathbf{m}}$ gives all the eigenstates with nonzero oscillator strength. In particular, the residue $f_\alpha(0)$ of Ψ_0 is basically the oscillator strength of the eigenstate α. The quantity $\langle \mathbf{m},0|\alpha\rangle = f_\alpha(\mathbf{m})/\langle\alpha|0,0\rangle$ yields information about the mutual electron-hole separation $\mathbf{m}$ of the electron-hole eigenfunction $|\alpha\rangle$ with a finite oscillator strength. The quantity $f_\alpha(\mathbf{m})$ is normalized in the sense

$$\sum_{\mathbf{m}} |f_\alpha(\mathbf{m})|^2 = f_\alpha(0). \tag{19}$$

Inserting Eq. (17) into Eq. (15), we obtain

$$\sum_{\mathbf{m}'} (\delta_{\mathbf{m},\mathbf{m}'} - K_{\mathbf{m},\mathbf{m}'} V_{\mathbf{m}'}) \Psi_{\mathbf{m}'} = \psi_{\mathbf{m}}, \tag{20}$$

where $\psi_{\mathbf{m}}$ was defined in Eq. (16) and

$$K_{\mathbf{m},\mathbf{m}'} = \sum_{\mathbf{k}} g(\mathbf{k},-\mathbf{k}) \cos(\mathbf{k}\cdot\mathbf{m}) \cos(\mathbf{k}\cdot\mathbf{m}') = \tfrac{1}{2}(\psi_{\mathbf{m}+\mathbf{m}'} + \psi_{\mathbf{m}-\mathbf{m}'}). \tag{21}$$

The expression in Eq. (20) is invariant under $\mathbf{m} \to -\mathbf{m}$ in view of $V_{\mathbf{m}'} = V_{-\mathbf{m}'}$. The solution $\Psi_{\mathbf{m}}$ is then obtained by inverting the matrix inside the parentheses on the left-hand side of Eq. (20). The time-dependent $\Psi_{\mathbf{m}}(t)$ is obtained from Eqs. (8) and (18):

$$\Psi_{\mathbf{m}}(t) = \frac{i}{2\pi} \int_{-\infty}^{\infty} \exp(-izt/\hbar) \Psi_{\mathbf{m}}(z) dz. \tag{22}$$

IV. OSCILLATOR STRENGTH

In this section, we study oscillator strengths for several interesting cases by solving Eq. (20). We study tunneling only between nearest-neighbor QDs in a direct-gap semiconductor with the energy dispersion

$$\varepsilon(\mathbf{k}) = -2 \sum_{\gamma} T_\gamma \cos a_\gamma k_\gamma, \tag{23}$$

where $T_\gamma = T_{\gamma e} + T_{\gamma h}$ is the net nearest-neighbor transfer integral in the γ direction and a_γ is the QD-lattice constant. We introduce a useful identity derived from Eqs. (12) (with $\mathbf{k}_e = -\mathbf{k}_h = \mathbf{k}$) and (23):

$$\psi_{\mathbf{0}}(z) = \sum_{\mathbf{k}} g(\mathbf{k},-\mathbf{k}) = -i \int_0^{\infty} \exp(i\tau z) \prod_{\gamma} J_0(\tau b_\gamma) d\tau, \tag{24}$$

where $b_\gamma = 2T_\gamma$ and $J_n(x)$ is the nth-order Bessel function. Note that the expression in Eq. (24) is independent of the sign of b_γ.

The quantity $\psi_m(z) \equiv \psi_m$ can readily be evaluated in one dimension, yielding

$$\psi_m = \frac{\theta(|z|-|b|)}{z\sqrt{1-(b/z)^2}} \left(\frac{z}{b} - \frac{z}{b}\sqrt{1-(b/z)^2} \right)^{|m|} + \frac{s(z)\theta(|b|-|z|)}{2i\sqrt{b^2-z^2}} \left\{ \left[\frac{z}{b} + i\sqrt{1-(z/b)^2} \right]^{|m|} + \text{c.c.} \right\}, \quad \text{(1D)}, \tag{25}$$

where $\theta(x)$ is the unit step function, and $s(z)$ is the sign of the infinitesimal imaginary part of z close to the real axis. In two dimensions, Eq. (24) yields for $b = b_x = b_y$

$$\psi_{\mathbf{0}} \equiv \psi_{\mathbf{0}}(z) = \frac{\theta(2|b|-|z|)}{|b|} \left\{ \frac{\text{sgn(z)}}{2} P_{-1/2}\left(1 - \frac{1}{2}(z/b)^2\right) + \frac{s(z)}{i\pi} Q_{-1/2}\left(1 - \frac{1}{2}(z/b)^2\right) \right\} + \frac{\theta(|z|-2|b|)}{|b|} \frac{\text{sgn(z)}}{\pi} Q_{-1/2}\left(\frac{1}{2}(z/b)^2 - 1\right), \quad \text{(2D)}, \tag{26}$$

where $\text{sgn}(z)$ is the sign of the real part of z and $P_n(x)$ ($Q_n(x)$) is the Legendre function of the first (second) kind. Only the real part is relevant for the last term of Eq. (26).

A. On-site Coulomb interaction

When the electron and the hole interact significantly only inside the same QD, namely for $V_{\mathbf{m}} = -U_0 \delta_{\mathbf{m},0}$, Eqs. (20) and (21) yield in all dimensions

$$\Psi_{\mathbf{0}} = \frac{\psi_{\mathbf{0}}}{1 + U_0 \psi_{\mathbf{0}}} \tag{27}$$

and

$$\Psi_{\mathbf{m}} = \frac{\psi_{\mathbf{m}}}{1 + U_0 \psi_{\mathbf{0}}}. \tag{28}$$

We first study Eq. (27) for a simple 1D QD lattice. Inserting Eq. (25) in Eq. (27), we find

$$\Psi_0(z) = \frac{\theta(|z|-|b|)}{z\sqrt{1-(b/z)^2}+U_0} + \frac{s(z)\theta(|b|-|z|)}{i\sqrt{b^2-z^2}+U_0}. \quad (29)$$

The quantity $\Psi_0(z)$ has a cut in the interval $-|b| \leqslant z \leqslant |b|$ representing the continuum band states and a simple pole at $z_0=-\sqrt{U_0^2+b^2}$, yielding near the pole

$$\Psi_0(z) \to \frac{R_0}{(z-z_0)}, \quad R_0 = \frac{U_0}{\sqrt{U_0^2+b^2}}. \quad (30)$$

This solution is in the form of Eq. (18) with $f_\alpha(0)=R_0$ for the ground state $\alpha=0$ and is consistent with the fact that an exciton bound state exists in one dimension, independent of the strength of the electron-hole attraction as is well known. The binding energy equals $\varepsilon_B=\sqrt{U_0^2+b^2}-|b|$ and is reduced from $\varepsilon_B=U_0$ of an isolated QD. The quantity Ψ_m is a measure of the amplitude for the electron-hole separation at a distance m as noted earlier in Sec. III and is obtained from Eq. (28), yielding at the resonance $z=z_0$

$$\Psi_m \to \frac{R_0[-\mathrm{sgn(b)}]^{|\mathrm{m}|}\exp(-|\mathrm{m}|/\xi)}{(z-z_0)} \equiv \frac{f_0(m)}{z-z_0}, \quad (31)$$

where

$$\xi = -\{\ln[\sqrt{(U_0/b)^2+1}-|U_0/b|]\}^{-1}. \quad (32)$$

Here, ξ is approximately the radius of the ground-state exciton wave function. It should be noted that, for the ground sublevels of the QDs under consideration in this paper, the sign of b is negative, indicating naturally that the exciton ground state has no node. The normalization $\Sigma_m|f_0(m)|^2 = f_0(0)=R_0$ is satisfied in Eq. (31) as proved in Eq. (19) in general.

We transform $\Psi_0(z)$ into the time space for the 1D lattice inserting Eq. (29) in Eq. (22) and integrating on the complex z plane

$$\Psi_0(t) = R_0\exp(-iz_0t/\hbar) + \frac{2}{\pi}\int_0^1 \frac{\sqrt{1-x^2}\cos(x\tau)}{(U_0/b)^2+1-x^2}dx, \quad (33)$$

where $\tau=bt/\hbar$. Two cases of limiting behavior are of interest. At $t=0$, the second term on the right-hand side of Eq. (33) yields $1-R_0$ and therefore $\psi_0(0)=1$ as expected. For $U_0=0$, we find

$$\Psi_0(t) = J_0(\tau) \to \sqrt{\frac{2}{\pi\tau}}\cos\left(\tau-\frac{1}{4}\pi\right), \quad (34)$$

where the arrow indicates the long-time ($\tau \gg 1$) behavior, for the time much longer than the nearest-neighbor tunneling time. In this case, the probability function $|\Psi_0(t)|^2$ decays as $1/t$ due to band motion as expected in the absence of electron-hole binding. In order to study the long-time behavior for $U_0>0$, we carry out the integration in Eq. (33) and find

$$\Psi_0(t) = R_0\exp(-iz_0t/\hbar) + \frac{1}{(U_0/b)^2+1} \times \sum_{n=0}^{\infty}\left[\frac{-d^2/d\tau^2}{(U_0/b)^2+1}\right]^n [J_1(\tau)/\tau].$$

At a sufficiently long time $\tau \gg 1$, only the $n=0$ contribution is important in the above summation, yielding

$$\Psi_0(t) = R_0\exp(-iz_0t/\hbar) + \sqrt{\frac{2}{\pi}}\frac{\cos\left(\tau-\frac{3}{4}\pi\right)}{\tau^{3/2}[(U_0/b)^2+1]}. \quad (35)$$

Here, the decay to the bound state is faster than in Eq. (34).

In 2D QD lattices, the continuum band extends over the energy range $-2|b|<z<2|b|$ as shown by the imaginary part in Eq. (26) representing a cut $\propto s(z)$ in this range. An example of a 2D lattice is InAs QDs grown in $GaAs/Al_xGa_{1-x}As$ quantum wells. The resonance energy exists only for $z<-2|b|$ and is given by the pole of

$$\Psi_{\mathbf{0}}(z) = \frac{|b|^{-1}}{\frac{U_0}{|b|} - \left\{\frac{1}{\pi}Q_{-1/2}\left(\frac{1}{2}-(z/b)^2-1\right)\right\}^{-1}}, \quad z<-2|b| \quad (36)$$

obtained by inserting the last term of Eq. (26) in Eq. (27). A numerical study of the properties of the pole of Eq. (36) will be given later in Sec. V.

The result in Eq. (31) can be extended to two and three dimensions analytically for the case $U_0 \gg |b_\gamma|$. This condition prevails often in typical QD structures where tunneling between QDs is small. Noting that the resonance energy is near $z=z_0\sim -U_0$ in this case, $g(\mathbf{k},-\mathbf{k})$ can be written to the first order in b_γ/U_0 as

$$g(\mathbf{k},-\mathbf{k}) = \frac{z^{D-1}}{N}\prod_\gamma g_\gamma(\mathbf{k},-\mathbf{k}), \quad g_\gamma(\mathbf{k},-\mathbf{k}) = \frac{1}{z-\varepsilon_\gamma(k_\gamma)}. \quad (37)$$

Here, $\varepsilon_\gamma(k_\gamma)=-b_\gamma\cos(k_\gamma)$ is the energy dispersion in the γ direction and D is the dimension. Employing $\cos(\mathbf{k}\cdot\mathbf{m}) = [\exp(i\mathbf{k}\cdot\mathbf{m})+\exp(-i\mathbf{k}\cdot\mathbf{m})]/2$, we can transform the $\mathbf{k}$ sum in the numerator of Eq. (28) into the product of the k_γ sums using the relationship in Eq. (37). We find at the resonance $z=z_0$

$$\Psi_{\mathbf{m}} \to \frac{R_0\prod_\gamma[-\mathrm{sgn(b}_\gamma)]^{|\mathrm{m}_\gamma|}\exp(-|\mathrm{m}_\gamma|/\xi_\gamma)}{(z-z_0)} = \frac{f_0(\mathbf{m})}{z-z_0}, \quad (38)$$

where

$$\xi_\gamma^{-1} = \ln\frac{2U_0}{|b_\gamma|} \quad (39)$$

and $R_0=1-\frac{1}{2}\Sigma_\gamma(b_\gamma/U_0)^2$ and $z_0=-U_0-\frac{1}{2}\Sigma_\gamma b_\gamma^2/U_0$. These results agree with the 1D case studied above in the limit U_0

$\geqslant |b|$. The normalization $\Sigma_{\mathbf{m}}|f_0(\mathbf{m})|^2 = f_0(0) = R_0$ is still satisfied in Eq. (38) for the ground state $\alpha = 0$

We now investigate the effect of extended Coulomb interaction by studying the effect of nearest-neighbor Coulomb interaction in one and two dimensions.

B. Extended Coulomb interaction in a 1D lattice

In a 1D lattice, we rewrite Eq. (20) in *general* as

$$\sum_{m'=0}^{\infty} [\delta_{m,m'} - (2 - \delta_{m',0})K_{m,m'}V_{m'}]\Psi_{m'} = \psi_m, \quad m \geqslant 0, \tag{40}$$

where use is made of the inversion-symmetry property of Ψ_m and ψ_m. A numerical study of some interesting examples of long-range electron-hole attraction will be studied later in Sec. V. In the following, we first consider on-site plus nearest neighbor attraction: $V_0 = -U_0$, $V_{\pm 1} = -U_1$, and $V_m = 0$ for $|m| > 1$. In this case, Eq. (40) yields

$$(1 - K_{0,0}V_0)\Psi_0 - 2K_{0,1}V_1\Psi_1 = \psi_0 \tag{41}$$

and

$$-K_{1,0}V_0\Psi_0 + (1 - 2K_{1,1}V_1)\Psi_1 = \psi_1. \tag{42}$$

We can rewrite $K_{0,0} = \psi_0$, $K_{0,1} = \psi_1$, and $K_{1,1} = (\psi_0 + \psi_2)/2$ in view of Eq. (21). Here, ψ_0 is given in Eq. (25). The resonance energy $z_0 < -|b|$ is obtained from pole of $\Psi_0(z)$ using $\psi_1 = zb^{-1}\psi_0 - b^{-1}$, $\psi_2 = (2z^2b^{-2} - 1)\psi_0 - 2zb^{-2}$ obtained from Eq. (16) or Eq. (25). We find

$$\Psi_0 = \frac{1}{|b|}\frac{1 + 2zu_1 - 2u_1(|b|\psi_0)^{-1}}{u_0 + 2zu_0u_1 + 2z^2u_1 + (1 - 2u_0u_1 - 2zu_1)(|b|\psi_0)^{-1}}, \tag{43}$$

where $u_0 = U_0/|b|$, $u_1 = U_1/|b|$ and z is in units of $|b|$. All other Ψ_m's ($|m| > 0$) are readily obtained in terms Ψ_0 through Eqs. (40)–(42). Numerical solutions for a general form of interaction will be considered later. Defining the denominator of Eq. (43) as D, $z = -\cosh\eta$, $\zeta = \exp(-\eta)$, and using Eq. (25), the bound-state energies are found from

$$D\zeta = \left[u_1\zeta^3 + \left(\tfrac{1}{2} - 2u_0u_1\right)\zeta^2 + (u_0 + u_1)\zeta - \tfrac{1}{2}\right] = 0,$$

yielding up to three roots. This solution is equivalent to that obtained by Ishida *et al.*[23]

C. Extended Coulomb interaction in a 2D square lattice

For on-site plus nearest-neighbor interaction in a 2D square lattice, Eq. (20) yields, after using various symmetry properties in Eqs. (15), (16), and (21) discussed earlier

$$(1 - K_{\mathbf{0},\mathbf{0}}V_0)\Psi_{\mathbf{0}} - 4K_{\mathbf{0},\mathbf{1}}V_1\Psi_{\mathbf{1}} = \psi_{\mathbf{0}} \tag{44}$$

and

$$-K_{\mathbf{1},\mathbf{0}}V_0\Psi_{\mathbf{0}} + (1 - 2K_{\mathbf{1},\mathbf{1}}V_1 - 2K_{\mathbf{1},\mathbf{y}}V_1)\Psi_{\mathbf{1}} = \psi_{\mathbf{1}}. \tag{45}$$

Here, the subscript $\mathbf{1}$ for $\Psi_{\mathbf{1}}$ and $\psi_{\mathbf{1}}$ indicates the four equivalent sites which are nearest neighbors to the origin at $\mathbf{0}$. Vectorial indices employed for $K_{\mathbf{m},\mathbf{m}'}$ signify $\mathbf{0} = (0,0)$, $\mathbf{1} = (1,0)$ and $\mathbf{y} = (0,1)$. The K matrices in Eqs. (44) and (45) are evaluated using Eqs. (12), (15), (16), (21), and (23) and are given by $K_{\mathbf{0},\mathbf{0}} = \psi_{\mathbf{0}}$ [cf. Eq. (26)], $K_{\mathbf{1},\mathbf{0}} = \psi_{\mathbf{1}} = (z\psi_{\mathbf{0}} - 1)/2b$,

$$K_{\mathbf{1},\mathbf{y}} = \frac{i}{|b|}\int_0^{\infty} \exp(i\tau z/|b|)J_1(\tau)^2 d\tau, \tag{46}$$

and $K_{\mathbf{1},\mathbf{1}} = z^2\psi_{\mathbf{0}}/2b^2 - z/2b^2 - K_{\mathbf{1},\mathbf{y}}$. The quantity $\Psi_{\mathbf{0}}$ is then given from Eqs. (44) and (45) by

$$\Psi_{\mathbf{0}} = \frac{1}{|b|}\frac{1 + zu_1 - u_1/(|b|\psi_{\mathbf{0}})}{u_0 + zu_0u_1 + z^2u_1 + (1 - u_0u_1 - zu_1)/(|b|\psi_{\mathbf{0}})}. \tag{47}$$

The quantity $K_{\mathbf{1},\mathbf{y}}$ is cancelled out from the second term in Eq. (45) and does not appear in the final result in Eq. (47). This expression reduces to the on-site interaction result in Eq. (27) for $u_1 = 0$.

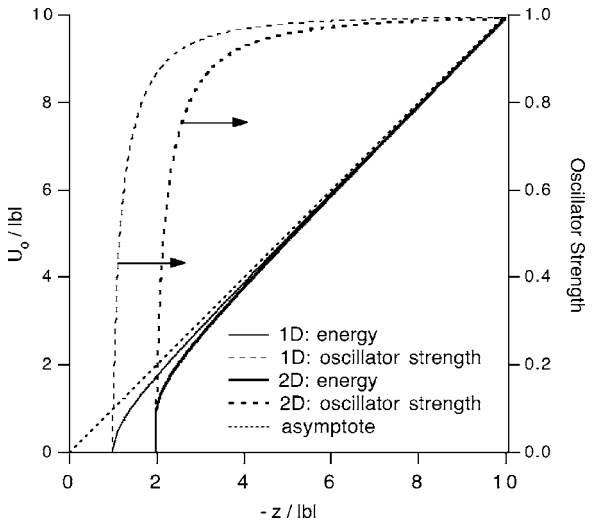

FIG. 1. Bound-state energy ($z < 0$) below the center of the band ($z = 0$) vs on-site interaction (U_0) (solid curves, left axis) and the oscillator strength vs the bound-state energy (dashed curves, right axis) in 1D (thin curves) and 2D (thick curves) lattices with band widths $2|b|$ and $4|b|$, respectively. The dotted curve is the asymptote.

V. NUMERICAL EVALUATION AND DISCUSSIONS

A. On-Site interaction in 1D and 2D lattices

Figure 1 displays the relationship between the on-site U_0 and the bound-state energy ($z < 0$), measured from the band center at $z = 0$ (solid curves, left axis). The right axis shows the oscillator strength versus the bound-state energy (dashed curves, right axis). These curves are obtained from Eqs. (30) and (36), respectively, for 1D (thin curves) and 2D (thick curves) lattices, with band widths $2|b|$ and $4|b|$. There exists only one bound state in each case, which appears from the bottom of the band for small $U_0/|b|$. The asymptotic behavior of the bound-state energy for $U_0/|b| \gg 1$ is given by $z = -U_0$ (dotted curve) as expected. In this limit, the oscillator

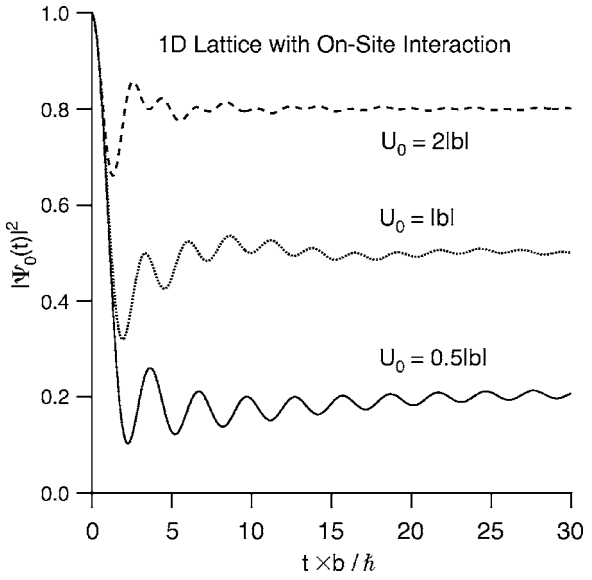

FIG. 2. Time-dependent behavior of $|\Psi_0(t)|^2$ for $U_0=0.5|b|$ (solid curve), $U_0=|b|$ (dotted curve), and $U_0=2|b|$ (dashed curve) in a 1D lattice with on-site attraction U_0 and bandwidth $2|b|$.

strength saturates to the full strength. The 1D result is consistent with the earlier numerical result obtained for a long chain.[22] The steep rise of the thick solid curve for the 2D case slightly below the band bottom follows $z \approx -2|b| - 32|b|\exp(-2\pi|b|/U_0)$ for $U_0 \ll |b|$ according to Eq. (36), meaning that a stronger U_0 is necessary to pull down a bound state below the bottom of the 2D continuum compared to the 1D case as expected. The rise is much slower in 1D (thin solid curve), in contrast, and follows $z-|b| \approx -0.5(U_0/b)^2$ for $U_0 \ll |b|$ according to Eq. (30).

In two dimensions, the connectivity is larger than in 1D, allowing the electron and the hole to dissociate from each other more easily. The thick curves in Fig. 1 show that a strong bound state emerges from the bottom of the band only when $U_0/|b|$ becomes larger than $\sim$ unity in 2D, where the oscillator strength jumps to 0.1 nearly abruptly but numerically continuously in a fine scale from zero. Experimentally, the photoluminescence (PL) intensity from the excitons in a 2D lattice will jump steeply and rise rapidly, saturating at a maximum value as the interdot lattice spacing increases for a constant U_0 (i.e., for the same QD size). In a 1D lattice, however, the PL intensity will rise continuously and rapidly without the sudden initial jump. A 2D lattice is formed by stacking 1D quantum-dot lattices for improved device efficiency. However, the above discussion indicates that the optical efficiency can drop drastically unless the QDs are kept far apart in a 2D lattice in such a way that the tunneling energy $|b|$ is small enough to assure sufficiently large $U_0/|b| > 1$. Strong long-range interaction (e.g., second-neighbor attraction) tends to diminish the above abrupt behavior for the electron-hole binding and the oscillator strength as will be shown later.

The time-dependent behavior of $|\Psi_0(t)|^2$ in Eq. (33) is shown in Fig. 2 for a 1D lattice for several values of $U_0/|b|$. The curves start with the value of unity initially and saturate at the asymptotic values of 0.2, 0.5 and 0.8, respectively for

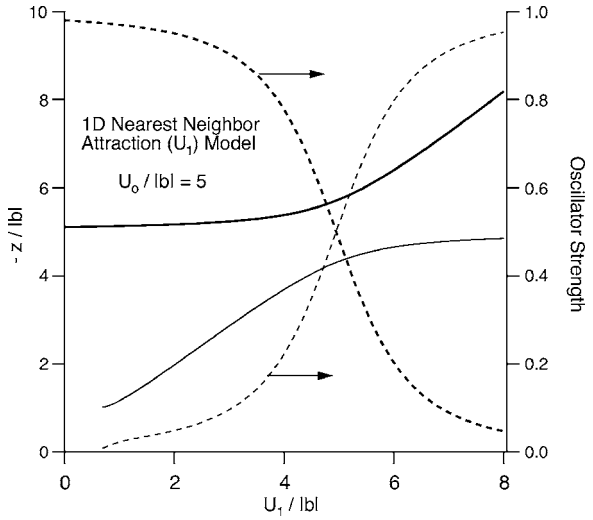

FIG. 3. Energies ($z<0$) of the two lowest bound states with nonzero oscillator strengths in a 1D lattice (solid curves, left axis) vs the nearest-neighbor attraction U_1. Here, $U_0=5|b|$ and $z=0$ at the center of the band of width $2|b|$. The oscillator strengths for the bound states are plotted on the right axis (dashed curves). The onset value of U_1 for the appearance of the upper bound state (thin solid curve) and its oscillator strength (thin dashed curve) is about $U_1=0.7|b|$. The thick curves represent the ground state.

$U_0=0.5|b|$ (solid curve), $U_0=|b|$ (dotted curve), and $U_0=2|b|$ (dashed curve) corresponding to R_0^2 in Eq. (30).

B. On-Site and nearest-neighbor attraction in a 1D lattice

In this case, more than one bound states are possible. The bound state energies and their oscillator strengths are calculated from Eq. (43). Figure 3 displays the energies of the two lowest symmetric bound states (solid curves, left axis) with nonzero oscillator strengths (dashed curves, right axis) for the on-site interaction $U_0=5|b|$ as a function of the nearest-neighbor attraction U_1. The oscillator strength of the ground state decreases with increasing U_1 because the nearest-neighbor sites steal the amplitude from $n=0$. The onset value of U_1 for the appearance of the upper bound state (thin solid curve) and its oscillator strength (thin dashed curve) is about $U_1=0.7|b|$. Experimentally, the effect of strong extended interaction U_1 as well as the long-range interactions to be discussed in Figs. 4 and 5 will give rise to a significant PL intensity from higher-energy levels. Near the unrealistic but interesting case of $U_1=U_0$, the two dashed curves cross owing to the fact that the ground state begins to have more amplitudes at sites $n=\pm 1$ away from $n=0$ for $U_1 > U_0$.

C. General attractive potential in a 1D lattice

A general 1D potential can be treated using Eq. (40). We study two cases here: a short-ranged exponentially decaying potential and a long-ranged Coulombic potential. An infinite number of bound states exists in this case. The exponential potential is of the form

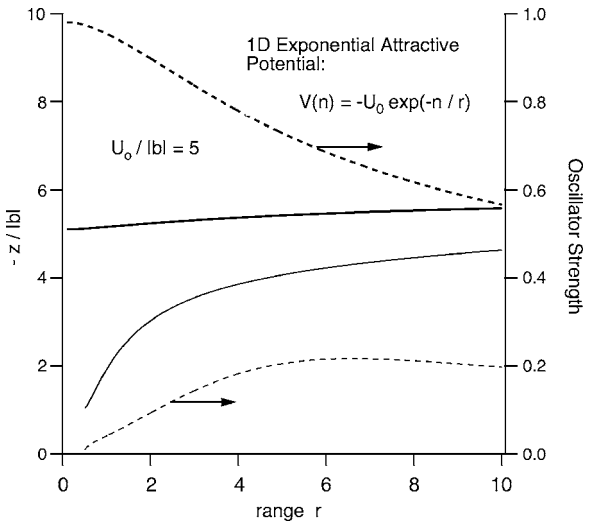

FIG. 4. Energies ($z<0$) of the two lowest bound states (solid curves, left axis) with nonzero oscillator strengths (dashed curves, right axis) for a 1D exponential attraction in Eq. (48) as a function of the range of the interaction. Here, $U_0=5|b|$ and $z=0$ at the center of the band of width $2|b|$. The onset range r for the upper bound state (thin solid curve) and its oscillator strength (thin dashed curve) is about $r=0.51$. The thick curves represent the ground state.

$$V(n) = -U_0 \exp(-n/r), \tag{48}$$

while the Coulombic potential is given by

$$V(n) = -\frac{U_0}{1+n/r}, \tag{49}$$

where the range r is in units of the lattice constant and $n=0,\pm1,\pm2,\ldots$. We study only the two lowest bound states with nonzero oscillator strengths (i.e., even parity).

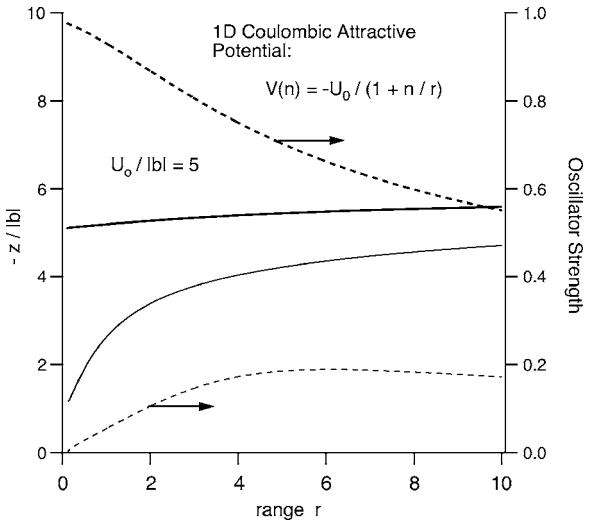

FIG. 5. Energies ($z<0$) of the two lowest bound states (solid curves, left axis) with nonzero oscillator strengths (dashed curves, right axis) for a 1D Coulombic attraction in Eq. (49) as a function of the range of the interaction. Here, $U_0=5|b|$ and $z=0$ at the center of the band of width $2|b|$. The onset range r for the upper bound state (thin solid curve) and its oscillator strength (thin dashed curve) is about $r=0.14$. The thick curves represent the ground state.

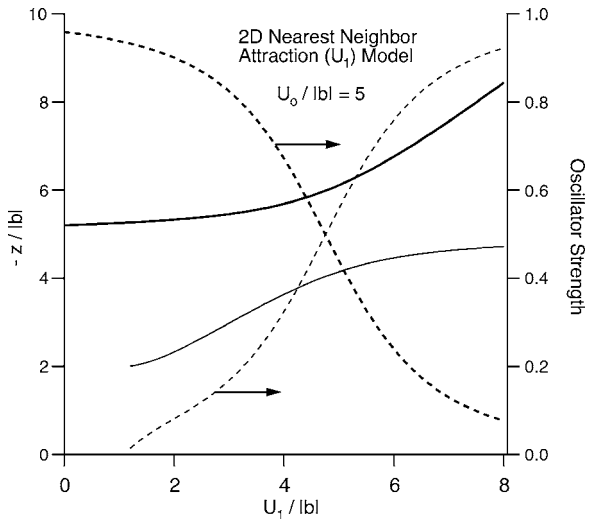

FIG. 6. Energies ($z<0$) of the two lowest bound states with nonzero oscillator strengths in a 2D square lattice (solid curves, left axis) vs the nearest-neighbor attraction U_1. Here, $U_0=5|b|$ and $z=0$ at the center of the band of width $4|b|$. The oscillator strengths for the bound states are plotted on the right axis (dashed curves). The onset value of U_1 for the appearance of the upper bound state (thin solid curve) and its oscillator strength (thin dashed curve) is about $U_1=1.2|b|$. The thick curves represent the ground state.

Figure 4 displays the energies of the two lowest even bound states (solid curves, left axis) and their oscillator strengths (dashed curves, right axis) from the exponential potential in Eq. (48) with the on-site interaction $U_0=5|b|$ as a function of r. The onset value of r for the appearance of the upper bound state (thin solid curve) and its oscillator strength (thin dashed curve) is about $r=0.51$.

Figure 5 shows the energies of the two lowest even bound states (solid curves, left axis) and their oscillator strengths (dashed curves, right axis) from the Coulombic potential in Eq. (49) with the on-site interaction $U_0=5|b|$ as a function of r. The onset value of r for the appearance of the upper bound state (thin solid curve) and its oscillator strength (thin dashed curve) is about $r=0.14$, much smaller than that of the exponential potential. This arises from the fact that the long-range Coulombic interaction allows the formation of an exciton with a large radius in contrast to the case of the exponential potential which cuts off the electron-hole interaction beyond a certain range. For the same reason, much more higher-energy bound states are found for Coulombic interaction than for the exponential potential. The results in Figs. 4 and 5 show reduced oscillator strength for the ground state for long-range interactions due to the increased exciton radius.

D. On-site and nearest-neighbor attraction in a square lattice

More than one bound states are possible in this case. Figure 6 displays the energies of the two lowest even bound states with nonzero oscillator strengths in a 2D square lattice (solid curves, left axis) calculated from Eq. (47) as a function of the nearest-neighbor attraction U_1. Here, $U_0=5|b|$ and

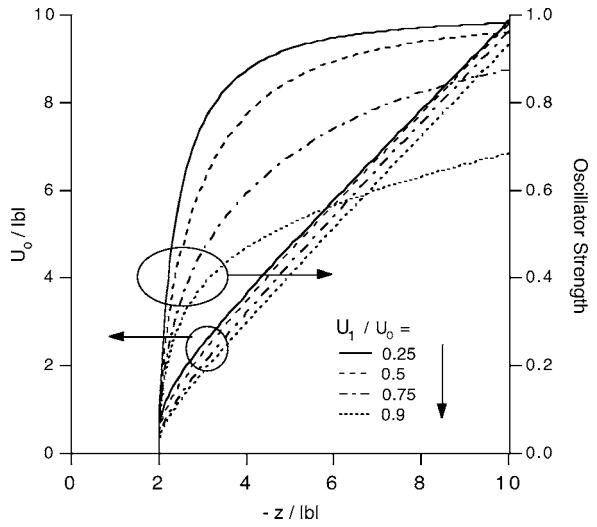

FIG. 7. Bound-state energy ($z<0$) below the center of the band ($z=0$) vs. on-site interaction (U_0) (left axis) and the oscillator strength vs the bound-state energy (right axis) in a 2D square lattice with band width $4|b|$ for several values of second-nearest-neighbor attraction U_1.

$z=0$ at the center of the band of width $4|b|$. The oscillator strengths for the bound states are plotted on the right axis (dashed curves). The onset value of U_1 for the appearance of the upper bound state (thin solid curve) and its oscillator strength (thin dashed curve) is about $U_1=1.2|b|$ which is much larger than $U_1=0.7|b|$ obtained for the 1D lattice in Sec. V B. Experimentally, this means that it is harder to observe PL lines from excited levels from a 2D lattice than from a 1D lattice with the same band-lattice parameters.

Figure 7 displays the relationship between the on-site U_0 and the ground bound-state energy for several values of the second-nearest-neighbor attraction U_1 for a square lattice (left axis). The right axis displays the oscillator strength for a given bound-state energy. The curves show that long-range interaction tends to diminish the abrupt behavior for the electron-hole binding and the oscillator strength in a 2D lattice discussed in Fig. 1. However, it should be noted that relatively strong $U_1/U_0>0.5$ is required to cause a significant deviation from the $U_1=0$ behavior shown in Fig. 1.

VI. CONCLUSIONS

We have studied excitonic binding of an electron and a hole interacting through an attractive potential in a tunnel-coupled quantum-dot lattice using a tight-binding model. The effect of interdot tunneling of the electron and the hole and their attraction on the exciton oscillator strength was assessed in 1D and 2D lattices. We examined general electron-hole attraction in 1D lattices and on-site and nearest-neighbor attraction in 2D square lattices. The time-dependent behavior of the oscillator strength was also examined for 1D on-site attraction. The present analysis shows that the reduction of the binding energy and the oscillator strength can be more drastic in 2D lattices than in 1D lattices for close packing of quantum dots, resulting in a reduced optical efficiency unless the quantum dots are kept sufficiently far apart for reduced inter-dot tunneling.

ACKNOWLEDGMENTS

Sandia is a multiprogram laboratory operated by Sandia Corporation, a Lockheed Martin Company, for the U.S. DOE under Contract No. DE-AC04-94AL85000.

*Present address: Sandia National Laboratories, Albuquerque, New Mexico 87185, USA.

[1] T. Takagahara, Phys. Rev. B **31**, 6552 (1985).
[2] A. Tomita, J. Shah, and R. S. Knox, Phys. Rev. B **53**, 10793 (1996).
[3] C. R. Kagan, C. B. Murray, M. Nirmal, and M. G. Bawendi, Phys. Rev. Lett. **76**, 1517 (1996).
[4] S. K. Lyo, Phys. Rev. B **62**, 13641 (2000); **64**, 201317 (2001).
[5] R. A. Kaindl, M. A. Carnahan, D. Hägelle, R. Lövenich, and D. S. Chemla, Nature (London) **423**, 734 (2003).
[6] J. Szczytko, L. Kappei, J. Berney, F. Morier-Genoud, M. T. Portella-Oberli, and B. Deveaud, Phys. Rev. Lett. **93**, 137401 (2004).
[7] S. Chatterjee, C. Ell, S. Mosor, G. Khitrova, H. M. Gibbs, W. Hoyer, M. Kira, S. W. Koch, J. P. Prineas, and H. Stolz, Phys. Rev. Lett. **92**, 067402 (2004).
[8] D. Y. Oberli, M.-A. Dupertuis, F. Reinhardt, and E. Kapon, Phys. Rev. B **59**, 2910 (1999).
[9] K. F. Karlsson, H. Weman, M.-A. Dupertuis, K. Leifer, A. Rudra, and E. Kapon, Phys. Rev. B **70**, 045302 (2004).
[10] D. Basko, G. C. La Rocca, F. Bassani, and V. M. Agranovich, Eur. Phys. J. B **8**, 353 (1999).
[11] M. Achermann, M. Petruska, S. Kos, D. L. Smith, D. D. Koleske, and V. L. Klimov, Nature (London) **429**, 642 (2004).
[12] X. Q. Li and Y. Arakawa, Phys. Rev. B **60**, 1915 (1999).
[13] T. Lundstrom, W. Schoenfeld, H. Lee, and P. M. Petroff, Science **286**, 2312 (1999).
[14] W. Que, Phys. Rev. B **45**, 11036 (1992).
[15] G. Lamouche and Y. Lépine, Phys. Rev. B **54**, 4811 (1996).
[16] G. S. Solomon, J. A. Trezza, A. F. Marshall, and J. S. Harris, Jr., Phys. Rev. Lett. **76**, 952 (1996).
[17] D. Bimberg, M. Grundmann, and N. N. Ledentsov, *Quantum Dot Heterostructures* (Wiley Press, New York, 1999).
[18] Z. M. Wang, K. Holmes, Yu. I. Mazur, and G. J. Salamo, Appl. Phys. Lett. **84**, 1931 (2004).
[19] M. V. Artemyev, A. I. Bibik, L. I. Gurinovich, S. V. Gaponenko, and U. Woggon, Phys. Rev. B **60**, 1504 (1999).
[20] B. Grandidier, Y. M. Niquet, B. Legrand, J. P. Nys, C. Priester, D. Stie'venard, J. M. Ge'rard, and V. Thierry-Mieg, Phys. Rev. Lett. **85**, 1068 (2000).
[21] G. W. Bryant, Physica B **314**, 15 (2002).
[22] G. W. Bryant, Phys. Rev. B **49**, 16129 (1994).
[23] K. Ishida, H. Aoki, and T. Chikyu, Phys. Rev. B **47**, 7594 (1993).
[24] K. Ishida, Phys. Rev. B **49**, 5541 (1994).

[25] W. Barford, R. J. Bursill, and R. W. Smith, Phys. Rev. B **66**, 115205 (2002).

[26] A. S. Davydov, *Quantum Mechanics* (Pergamon Press, New York, 1965), p. 103.

[27] J. A. Simmons, S. K. Lyo, N. E. Harff, and J. F. Klem, Phys. Rev. Lett. **73**, 2256 (1994).

[28] S. K. Lyo and J. A. Simmons, J. Phys.: Condens. Matter **5**, L299 (1993).